Oceanographic Measurement Conducted in the Mediterranean Sea - Toulon Bay

Students:
Hyejoo Kwon
Ahmed Borchani
Sahil Abdullayev
Anastasiia Frolova
Mukesh Sadhasivam
Akira Techapattaraporn
Godsfavour Ugwu-Gabriel
Seyed Amirhesaan Mirabolghasemi

Course Title: Introduction to Oceanography

Instructor:
Pr. Anne Molcard

Submitted on February 2, 2025

UNIVERSITÉ DE TOULON

MIR MARINE & MARITIME INTELLIGENT ROBOTICS

Contents

1 Introduction

On October 18, 2024, a field experiment was conducted in Toulon Bay, located on the southern coast of France. The main objective of this fieldwork was to collect data on underwater properties and the velocities of currents within the bay. The experiment comprised two key tasks: the use of a CTD sensor to measure variables such as oxygen, chlorophyll, temperature, and salinity, and the deployment of drifters to track their trajectories over time. To achieve these goals, three main locations were selected as anchoring points, where instruments were deployed and monitored. As illustrated in Figure 1, CTD measurements were conducted farther from the coastline, allowing the measurement of deeper water properties. In contrast, drifters were deployed closer to shore to avoid strong waves. The weather conditions during the experiment were clear, with temperatures ranging from 15°C to 21°C. Although the winds were mild, the waves were strong, likely due to storms that had occurred over past few days.

Figure 1: Main location points

As shown in Table 1, the CTD sensor was deployed twice, each deployment lasting approximately 20 minutes, reaching depths of 338 meters and 205 meters, respectively. In Chapter 2, temperature and salinity are identified as the primary properties for investigation, with an analysis of the collected data. Additionally, three drifters were released for approximately 90 minutes at certain points, as presented in Table 2. These drifters included two types: cylindrical and donut-shaped. Two of the drifters were equipped with anchors, while one was not. It was expected that the movement patterns of each drifter would vary based on their condition and shape. Chapter 3 will provide a comparison of their data and discuss the relationship between these movement patterns and the velocities of surface currents. Finally, the concluding chapter will summarize the key findings of this experiment and draw the overal conclusions.

Table 1: Details of CTD devices based on the handwriting paper

CTD	Start Time	Start Coordinates	End Time	End Coordinates	Depth
1	08:09 AM	43.0346°N, 6.0016°E	08:30 AM	43.0117°N, 6.0052°E	338m
2	08:43 AM	43.0205°N, 6.0077°E	09:00 AM	43.0205°N, 6.0054°E	205m

Table 2: Details of drifters based on the handwriting paper

D	Start Time	Start Coordinates	End Time	End Coordinates	Features
1	09:18 AM	43.0361°N, 5.5964°E	10:49 AM	43.0361°N, 5.5964°E	White, anchored
2	09:18 AM	43.0361°N, 5.5964°E	10:49 AM	43.0864°N, 5.5964°E	Yellow, anchored
3	09:18 AM	43.0361°N, 5.5964°E	11:02 AM	43.0452°N, 5.5961°E	White, unanchored

2 CTD

A CTD (Conductivity, Temperature, Depth) instrument is a key tool used in oceanography and marine science for measuring the physical and chemical properties of seawater. The CTD sensor is typically deployed in the water to gather high-resolution data about the temperature, salinity, and depth of the water at various depths. These measurements are crucial for understanding oceanographic conditions and marine ecosystems.

The components of a CTD are as follows:

- **Temperature**: Measured using a high-precision thermometer.
- **Salinity**: Measured through electrical conductivity, as conductivity increases with higher salinity. The relationship between conductivity and salinity is used to derive the salinity of the water.
- **Depth**: Measured using pressure sensors, which are often calibrated to provide the depth of the sensor in the water. In our practical example, python's library gsw was used to compute depth using pressure and latitude value.

The CTD was first submerged to a depth of 338m, as shown in Figure 2a. Later on, the CTD was deployed again at a different location to a depth of 205m, as depicted in Figure 2b. The CTD measures values during the downcast (going from the water surface down) and the upcast (from the deepest point the CTD reaches back to the water surface). In this study, the upcast data was used since it had less noise.

Figure 2 presents the CTD profile of temperature, salinity, density, and oxygen variation with water depth in the Mediterranean Sea from two measurements conducted in October 2024. Both measurements show a typical Mediterranean thermocline structure, with surface waters warmed by solar radiation and a rapid decrease in temperature with depth. However, the second measurement shows a deeper thermocline extending below 100 m, compared to around 50 m in the first measurement. This difference may indicate localized variations in atmospheric conditions (e.g., wind or heat flux) or the influence of regional currents. The stable temperatures below 150 m in both profiles (14°C) represent the homogenous deep water of the Mediterranean Sea.

The salinity profiles in both graphs demonstrate high salinity typical of the Mediterranean Sea, driven by evaporation exceeding freshwater inputs. The second measurement shows higher salinity at the surface (38.4 PSU) compared to the first (38.3 PSU). Additionally, the halocline in the second profile extends deeper, reaching maximum salinity (38.65 PSU) below 150 m, whereas in the first profile, salinity stabilizes earlier (38.55 PSU at 100 m). These differences suggest variability in mixing processes or water mass characteristics.

The density gradients closely follow the combined effects of temperature and salinity. The second measurement exhibits greater density at depth (over 1030 kg/m^3) than the first (up to 1029.5 kg/m^3), reflecting the impact of increased salinity and a deeper halocline. Both profiles show stratified water columns, with density increasing rapidly between 50–150 m, which marks strong pycnoclines that inhibit vertical mixing.

Oxygen profiles differ more noticeably. In the first measurement, oxygen decreases steadily from 220 µmol/kg at the surface to 180 µmol/kg below 200 m. In the second measurement, oxygen declines more sharply after 100 m, reaching 170 µmol/kg below 300 m. This steeper gradient suggests reduced oxygen replenishment or higher biological activity leading to oxygen consumption in the second measurement location.

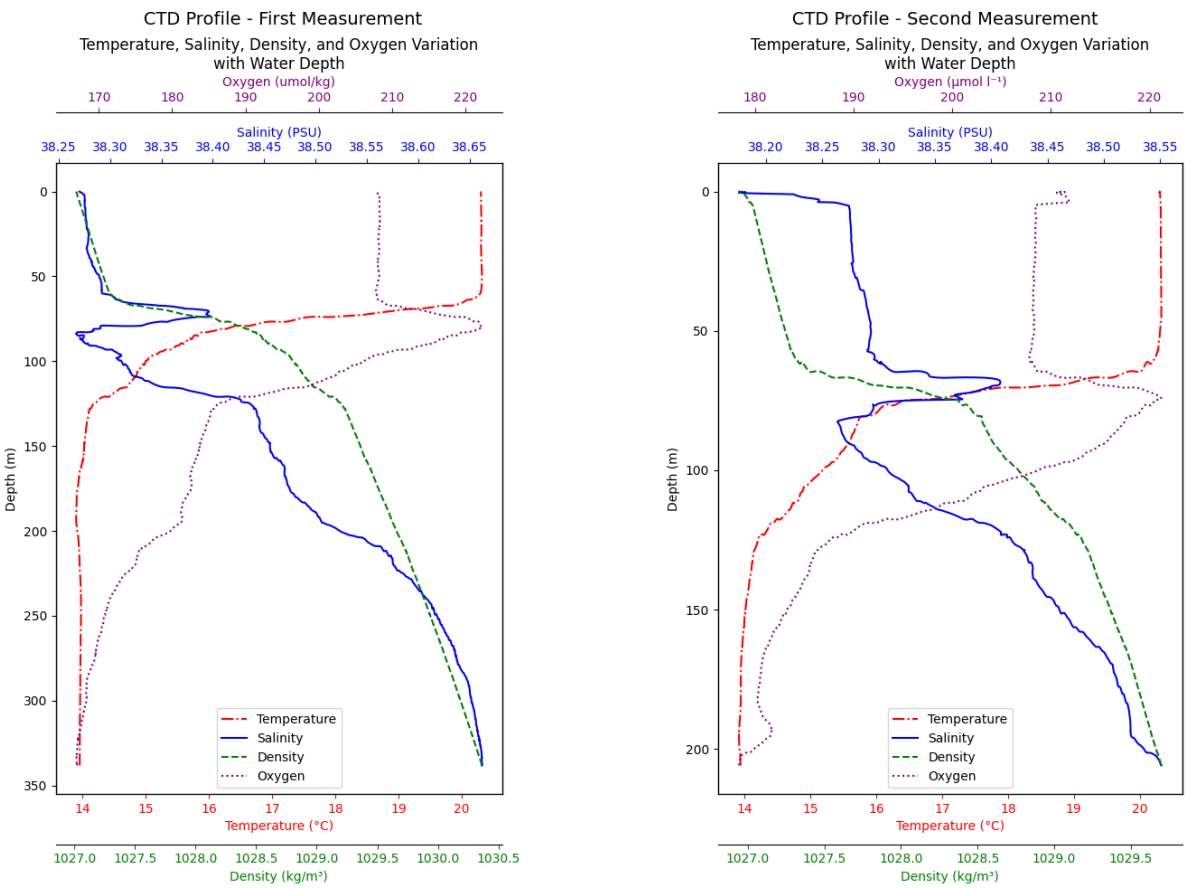

(a) First CTD measurement

(b) Second CTD measurement

Figure 2: Comparison of two CTD measurements

The differences between the two measurements may reflect localized hydrological and biological variations. Factors such as wind-driven mixing, freshwater input, evaporation rates, or the influence of regional water masses could account for the deeper thermocline, halocline, and pycnocline observed in the second measurement. Additionally, the sharper oxygen gradient in the second profile may be influenced by localized productivity, organic matter decomposition, or limited mixing in deeper waters.

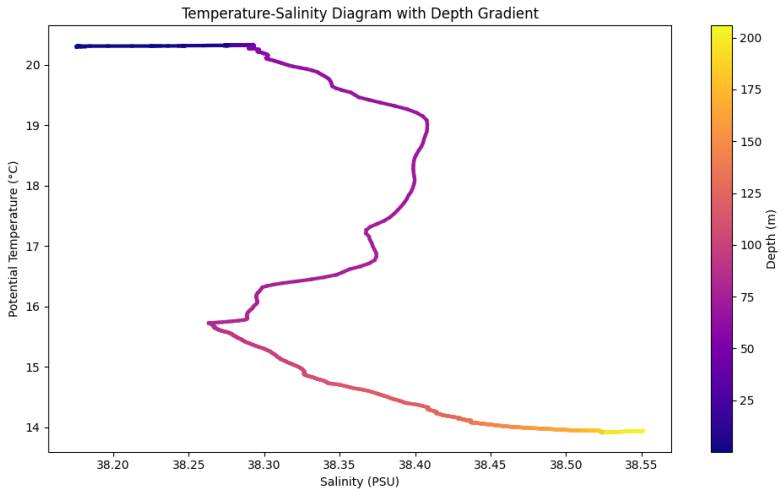

Figure 3: TS diagram of the Mediterranean Sea

Figure 3 illustrates the relationship between potential temperature (°C) and salinity (PSU) across depths, with the color gradient indicating depth (from 0 m at purple to 200 m at yellow). TS diagrams are a critical tool for identifying water masses and understanding ocean stratification, mixing, and circulation.

At the surface (0–50 m, purple), the potential temperature is high, around 20°C, and salinity is relatively low, approximately 38.3 PSU, reflecting the influence of atmospheric heating and limited evaporation during October, along with possible freshwater inputs. The nearly vertical line at the top of the TS curve indicates a well-mixed surface water column with minimal variation in salinity and temperature. Between 50–150 m, there is a sharp transition where temperature decreases rapidly, and salinity increases steadily. This corresponds to thermocline and halocline, creating a strong pycnocline that inhibits vertical mixing. The gradual slope of the TS curve in this depth range highlights the combined influence of temperature and salinity on water mass properties, with salinity becoming increasingly significant as temperature stabilizes. Below 150 m, the TS curve flattens, indicating stabilized potential temperature (14°C) and salinity (38.55 PSU), characteristic of the homogeneous deep-water mass typical of the Mediterranean, where mixing and circulation are limited. The high salinity in the deep water reflects the Mediterranean's unique hydrology, driven by high evaporation rates exceeding precipitation and riverine input, resulting in dense, saline deep waters.

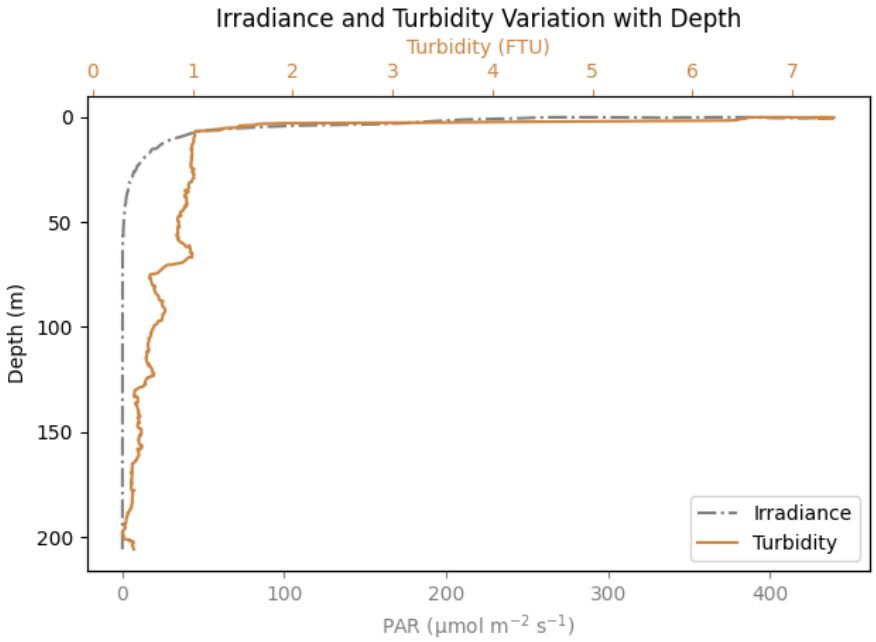

Figure 4: Depth profiles of irradiance and turbidity in the Mediterranean Sea

Figure 4 depicts the profiles of irradiance (PAR, Photosynthetically Active Radiation) and turbidity (FTU, Formazin Turbidity Units) with depth in the Mediterranean Sea for October 2024. The irradiance profile shows a rapid exponential decrease with depth, with the majority of light intensity absorbed in the upper 50 m of the water column. This sharp decline indicates the euphotic zone, where sufficient light supports photosynthesis, is confined to shallow depths due to the high attenuation of light by water and particulates. Beyond 100 m, irradiance approaches zero, marking the aphotic zone, where biological processes relying on light are no longer supported. The turbidity profile is relatively low throughout the water column, with values mostly below 7 FTU. Turbidity is slightly higher near the surface and shows small fluctuations down to 50 m, likely due to suspended particles, organic matter, or biological

activity such as phytoplankton blooms. Below 50 m, turbidity stabilizes and remains nearly constant, indicating minimal particulate matter or sedimentation influence in the deeper layers.

The relationship between irradiance and turbidity underscores the impact of suspended particles on light penetration. While turbidity values are not excessively high, even small concentrations of particulates can significantly attenuate light in the upper water column, as observed here. Seasonal influences such as reduced plankton activity or low sediment input in October likely contribute to the relatively low turbidity levels. This combination of low turbidity and rapid light attenuation suggests that water clarity is relatively good, yet the limited penetration of light reflects the typical properties of the Mediterranean, where the euphotic zone is shallow and constrained by natural light absorption properties of seawater. The stable turbidity values at depth indicate minimal vertical mixing, further emphasizing the stratified nature of the Mediterranean water column in this region and season.

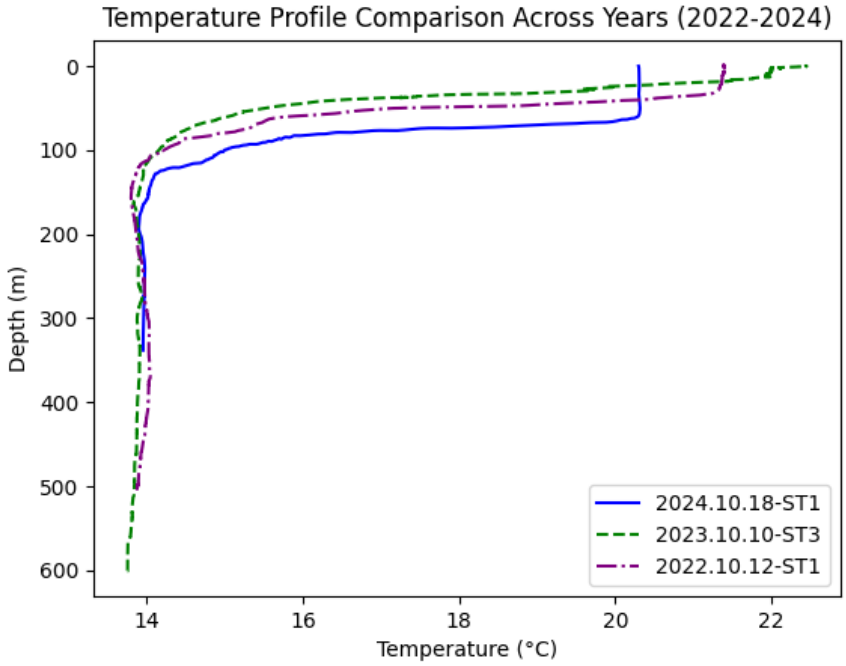

Figure 5: Comparison of temperature profiles across depths in recent years in the Mediterranean Sea

Figure 5 compares temperature profiles at different depths in the Mediterranean Sea for the three successive Octobers of 2022, 2023, and 2024. The comparison highlights the annual variability in the thermal structure of the water column and provides insights into both surface and subsurface temperature patterns. The surface temperature is cooler in 2024, around 20°C, compared to the other two years, suggesting potentially lower atmospheric temperatures, increased wind-driven mixing, or enhanced cooling effects during October 2024. In contrast, 2023 shows the highest surface temperature, approximately 22°C, indicating strong surface heating, minimal mixing, or calmer atmospheric conditions that allowed for greater heat retention. Meanwhile, 2022 exhibits an intermediate surface temperature of around 21°C, which reflects moderate surface heating and stratification compared to the conditions in 2023 and 2024.

The thermocline is shallower and more pronounced in 2024, starting near 50 m and extending to around 100 m, which indicates enhanced vertical mixing or cooler conditions that create sharper temperature gradients at shallower depths. In contrast, 2023 exhibits a deeper

and more gradual thermocline, stretching from 50 m to beyond 150 m, which suggests strong stratification with limited vertical mixing that allows warmer waters to persist at greater depths. Meanwhile, in 2022, the thermocline depth is similar to 2024 but slightly deeper, stabilizing around 150 m, which reflects a balance between mixing and stratification.

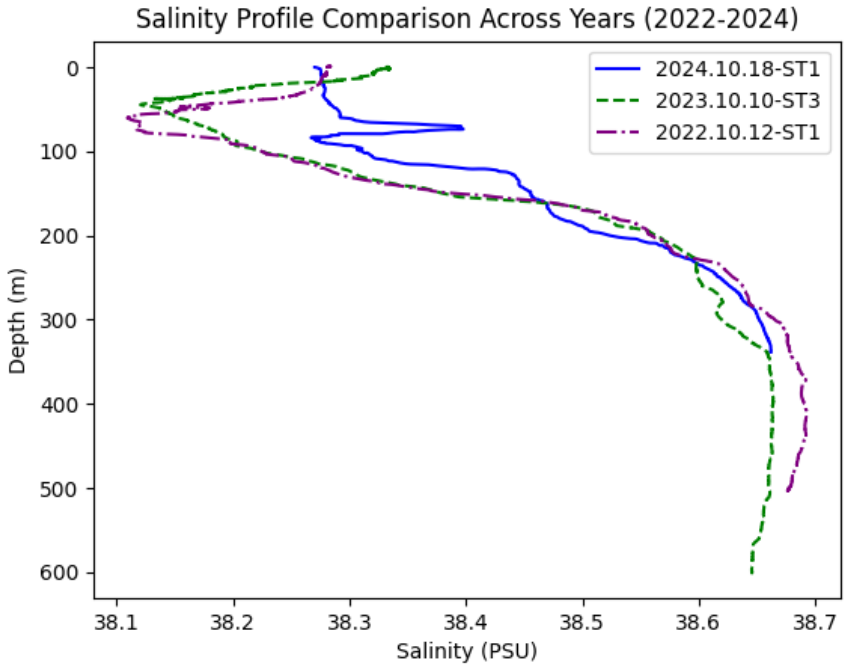

Figure 6: Comparison of salinity profiles across depths in recent years in the Mediterranean Sea

Figure 6 compares salinity profiles at different depths in the Mediterranean Sea for the three successive Octobers of 2022, 2023, and 2024. The salinity values, measured in PSU (Practical Salinity Units), show variations in surface and subsurface layers that reflect the influence of evaporation, freshwater input, and vertical mixing.

The surface salinity is around 38.3 PSU in 2024, lower than in 2023 but slightly higher than in 2022, which suggests a balance between evaporation and localized freshwater input or mixing. In 2023, the highest surface salinity, approximately 38.4 PSU, is observed, likely driven by stronger evaporation or reduced freshwater input, which indicates more arid or less turbulent atmospheric conditions compared to other years. Meanwhile, in 2022, the surface salinity is the lowest, at around 38.25 PSU, which reflects a greater freshwater influence or reduced evaporation during this period.

The halocline is prominent between 50–150 m in 2024, with salinity rising from approximately 38.3 PSU to 38.6 PSU and stabilizing below 150 m. This well-defined halocline indicates stratification with limited vertical mixing. In contrast, 2023 shows a more gradual salinity increase with depth, which reaches about 38.65 PSU below 200 m that suggests a weaker halocline and stronger vertical mixing or the intrusion of more saline water masses. Meanwhile, in 2022, the salinity profile is similar to 2024 but with a less pronounced halocline, which stabilizes at around 38.6 PSU below 150 m that reflects intermediate mixing conditions compared to 2023 and 2024.

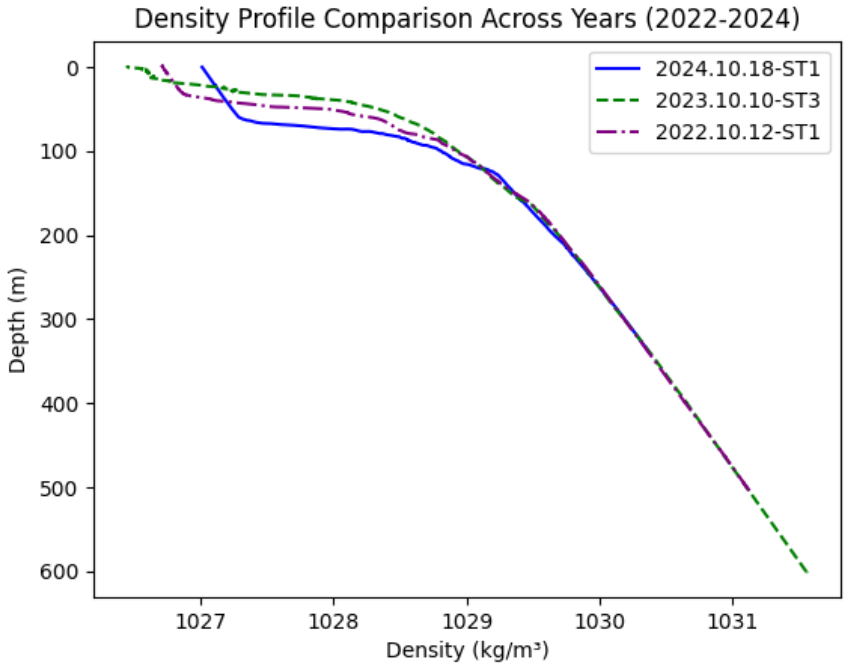

Figure 7: Comparison of density profiles across depths in recent years in the Mediterranean Sea

Figure 7 compares density profiles at different depths in the Mediterranean Sea for the three successive Octobers of 2022, 2023, and 2024. The density variations with depth reflect the combined effects of temperature and salinity, with denser water generally corresponding to cooler and more saline conditions.

The surface density is around 1027 kg/m^3 in 2024, slightly higher than in 2023 but lower than in 2022, which reflects a combination of cooler surface temperatures and moderately high salinity. In 2023, the surface density is the lowest among the three years, approximately 1026.7 kg/m^3, driven by higher surface temperatures and reduced salinity, both of which decrease density. Meanwhile, in 2022, the highest surface density, about 1027.2 kg/m^3, is observed, likely due to lower surface temperatures and slightly lower salinity than in 2024, with the colder water contributing to the increased density.

The pycnocline, where density increases most rapidly with depth, is observed between 50–150 m in 2024, corresponding to thermocline and halocline in the temperature and salinity profiles. This indicates strong stratification that limits vertical mixing. In 2023, the pycnocline is deeper and more gradual, with density increasing steadily beyond 150 m, which reflects weaker stratification and greater mixing or water mass exchange that aligns with the deeper thermocline seen in the temperature profile. In 2022, the pycnocline is similar to 2024 but slightly deeper, which stabilizes around 200 m that suggests intermediate stratification with some mixing but less than in 2023.

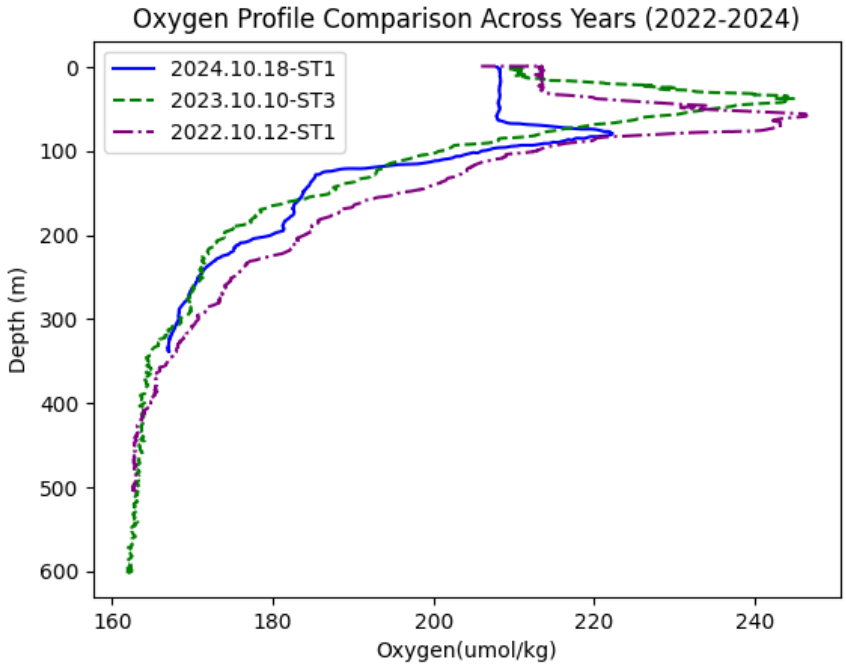

Figure 8: Comparison of oxygen profiles across depths in recent years in the Mediterranean Sea

Figure 8 compares oxygen profiles at different depths in the Mediterranean Sea for the three successive Octobers of 2022, 2023, and 2024. Oxygen levels reflect biological activity, vertical mixing, and water mass characteristics, which offers insights into the physical and biochemical processes at play.

Surface oxygen concentrations are slightly higher, around 240 µmol/kg in 2024, compared to 2023 and 2022. This may be due to increased atmospheric exchange or enhanced primary production that is potentially driven by cooler temperatures or localized wind-driven mixing. In 2023, surface oxygen levels are slightly lower, approximately 230 µmol/kg, than in 2024 but higher than in 2022, which possibly reflects reduced mixing or warmer surface temperatures that decrease oxygen solubility. In 2022 (purple line), surface oxygen concentrations are the lowest, around 225 µmol/kg, which could indicate reduced photosynthetic activity or limited atmospheric oxygen exchange during that period.

The decline in oxygen levels with depth is more gradual in 2024b compared to other years, with concentrations steadily decreasing to around 190 µmol/kg below 200 m. This suggests better oxygenation at intermediate depths, potentially due to localized mixing or the presence of a younger water mass. In 2023, oxygen levels drop sharply between 100–200 m, stabilizing at approximately 180 µmol/kg below 200 m. This steep gradient indicates limited oxygen replenishment at intermediate depths, likely due to weaker mixing or stronger stratification. In 2022, the oxygen profile shows a decline similar to 2023 but stabilizes at slightly higher levels, around 185 µmol/kg below 200 m, which reflects intermediate conditions with moderate mixing and biological consumption at depth.

3 Drifters

Drifters are devices used to measure wave speed by tracking their movement over time. They provide valuable data on surface currents and wave dynamics, playing a crucial role in marine and coastal studies.

Three drifters of different configurations were deployed in the study area to measure wave speed. The deployment details are as follows:

- **Drifter 1**: The first drifter, identified by its yellow color, was deployed at 09:18:00 and collected at 10:49:00. It started at the initial position of 43.07865° latitude and 5.98442° longitude and drifted to its final position at 43.07603° latitude and 5.98523° longitude.
- **Drifter 2**: The second drifter, which was white, was deployed simultaneously with the first and was collected at 10:45:00. Its initial position was 43.07504° latitude and 5.98469° longitude, and its final position was 43.07913° latitude and 5.98422° longitude.
- **Drifter 3**: The last drifter, a white unit without an anchor, was deployed at the same time as the others and was collected later at 11:02:00. It started at 43.07512° latitude and 5.99315° longitude, drifting to its final position at 43.07916° latitude and 5.98429° longitude.

The distinct configurations of the drifters (color and presence of an anchor) provide an opportunity to analyze their performance and the effect of design differences on drift patterns. The movement data collected will help in understanding the surface currents and wave dynamics in the study area.

3.1 Drifter Position

Three drifters were deployed at approximately the same location and were retrieved on the return trip. The graph illustrates the paths and velocities of each drifter. Although all drifters were initially released together, their subsequent movement patterns differed significantly, highlighting the influence of wind and anchoring on their trajectories. Below is the plot showing the positions of marine drifters:

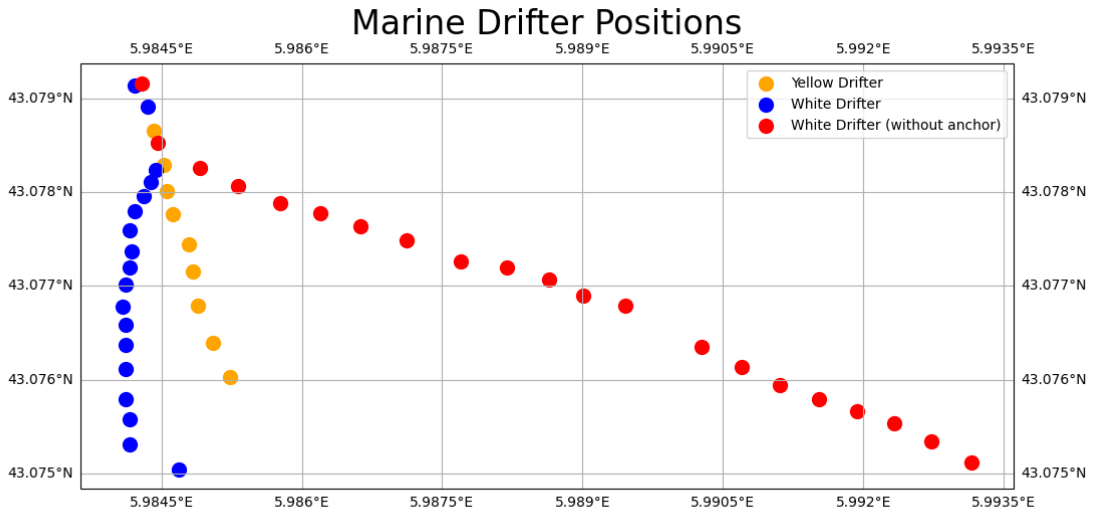

Figure 9: Marine Drifter Positions

As shown in Figure 9, the drifter positions are distributed along the coastline. The first, second, and third drifters are marked in orange, blue, and red, respectively.

The distances traveled by the drifters were calculated using the Haversine formula, which is widely used to compute the great-circle distance between two points on a sphere. The Haversine formula calculates the great-circle distance d between two points (ϕ_1, λ_1) and (ϕ_2, λ_2) on a sphere with radius R:

$$d = 2R \arcsin\left(\sqrt{\sin^2\left(\frac{\phi_2 - \phi_1}{2}\right) + \cos(\phi_1)\cos(\phi_2)\sin^2\left(\frac{\lambda_2 - \lambda_1}{2}\right)}\right) \tag{1}$$

where:

- ϕ_1, ϕ_2 are the latitudes in radians.
- λ_1, λ_2 are the longitudes in radians.
- R is the Earth's radius, approximated as 6371 km.

Using the Haversine formula, the distances traveled by each drifter were computed and presented in Table 3.

Table 3: Calculated distances traveled by drifters

	Initial Lat. and Long.	*Final Lat. and Long.*	*Distance (km)*	*Avg. Velocity (m/s)*
Drifter 1	(43.07865, 5.98442)	(43.07603, 5.98523)	0.299	0.06
Drifter 2	(43.07504, 5.98469)	(43.07913, 5.98422)	0.456	0.10
Drifter 3	(43.07512, 5.99315)	(43.07916, 5.98429)	0.848	0.15

Although all drifters were launched simultaneously, the distances covered by the three drifters varied significantly due to differences in design, anchoring, and wind influence.

Drifter386 (Yellow): Covered the shortest distance of 0.299 km, moving at the slowest velocity. This drifter was equipped with an anchor, which reduced its susceptibility to surface wind forces and allowed it to be more influenced by subsurface currents. The slower movement suggests that the anchor was effective in minimizing drift and maintaining its position relative to subsurface flows.

Drifter7160 (White, Anchored): Traveled 0.456 km, covering a medium range. Although also anchored, its circular shape likely allowed more interaction with surface winds compared to the yellow drifter, resulting in slightly faster movement. However, the anchor still provided significant resistance, restricting its drift speed compared to the unanchored drifter.

Drifter9931 (Unanchored White Drifter): Covered the greatest distance of 0.848 km and displayed the highest velocity. Without an anchor, this drifter was entirely at the mercy of surface wind forces, which drove it farther and faster than the anchored counterparts. Its circular design further amplified its wind susceptibility, leading to minimal resistance and greater displacement.

Moreover, the data collected on the 16th of October was analyzed and compared with that of the 18th of October, as shown in Figure 10. The comparison reveals a distinct difference in the drift patterns between the two dates. Specifically, the drifters deployed on the 16th of October exhibit a tendency to drift farther compared to those on the 18th of October. This observation suggests a variation in the environmental conditions, such as stronger currents or increased wave activity on the 16th, which could have influenced the drifters' movement. Such comparisons highlight the dynamic nature of the study area and emphasize the importance of temporal context when analyzing oceanographic data.

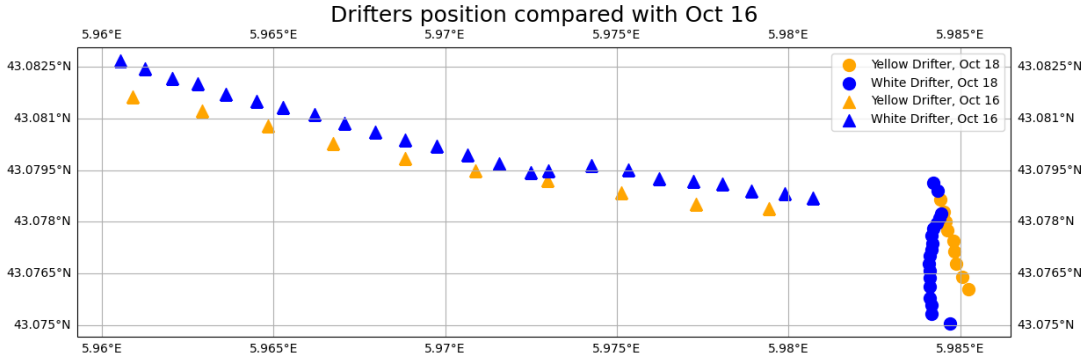

Figure 10: Drifter Position (October 16 and 18 Comparison)

3.2 Drifter Velocity

The velocity, expressed in meters per second (m/s), for each drifter was calculated using the Haversine formula (Equation 1) to convert the given longitude and latitude in degrees to meters and kilometers. This allowed for the accurate determination of the drifters' velocities over time.

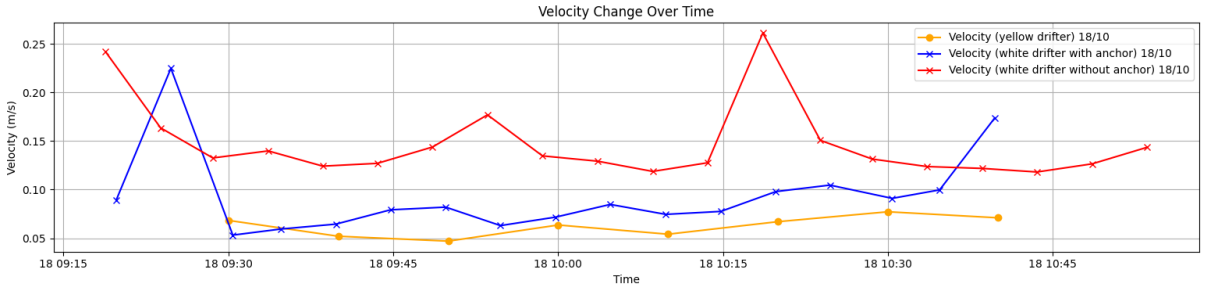

Figure 11: Velocity over Time (October 18)

Figure 11 shows the velocities of drifters. The average velocity for the yellow drifter was approximately 0.06 m/s, while the white drifter with an anchor had an average velocity of 0.10 m/s, and the white drifter without an anchor recorded 0.15 m/s.

These differences in velocities can be attributed to the shape of the equipment and the presence of an anchor. The yellow drifter, due to its shape, measured velocity below the surface and was less influenced by wind, resulting in the lowest velocity among all 3 drifters. In contrast, the white drifter without an anchor exhibited a higher velocity compared to the white drifter with an anchor, as it was more affected by surface winds, as shown in Figure 11.

There are several cases of increased velocities in Figure 11 that correspond to the drifters' positions shown in Figure 9. For example, the increased velocity of approximately 0.26 m/s at around 10:20 on October 18 coincides with the white drifter without an anchor moving further along the path from (43.0765, 5.9895) to (43.0762, 5.9900).

Another example is the increased velocity of approximately 0.18 m/s at around 10:40 on October 18 coincides with the white drifter with an anchor moving further along the path from (43.0755, 5.9830) to (43.075, 5.9850) and even changing the direction. A possible explanation for this change could be a shift in wind speed and direction, which affected the drifter's movement and caused the observed increase in velocity.

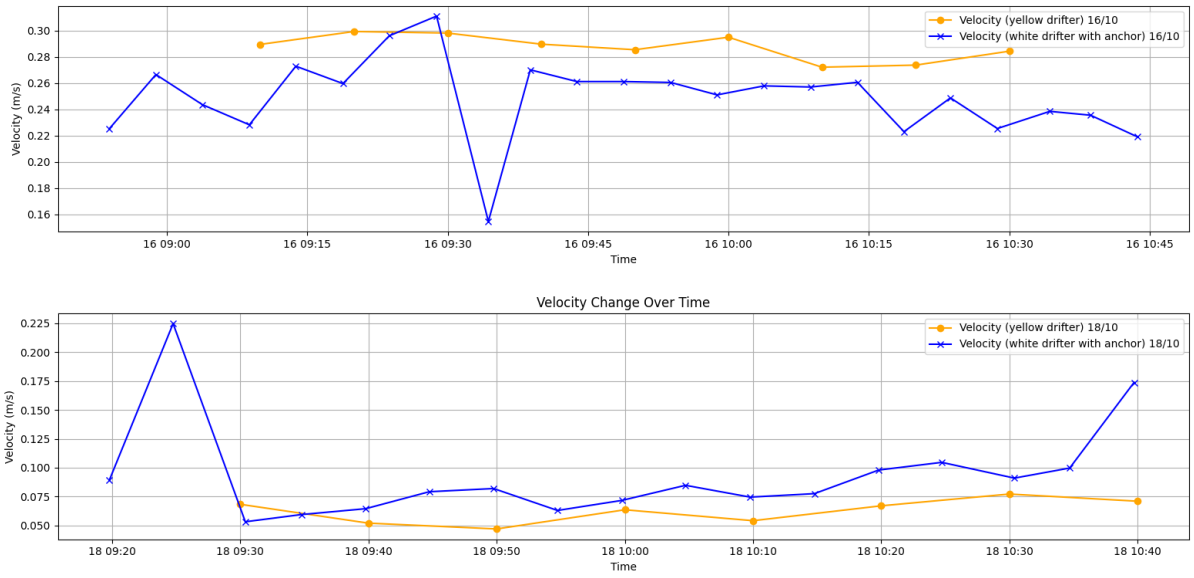

Figure 12: Velocity over Time (October 16 and October 18 comparison)

On October 16, the average velocity for the yellow drifter was 0.29 m/s, while the white drifter recorded an average velocity of 0.25 m/s.

These increased velocities can be attributed to the adverse weather conditions on that day. As shown in Figure 12, stronger winds and higher waves on October 16 caused the drifters to move faster compared to the calmer conditions observed on October 18. The significant velocity difference between the two dates highlights the impact of the differences in wind speed and, consequently, waves and current velocity, as shown in Figure 13 and Figure 14.

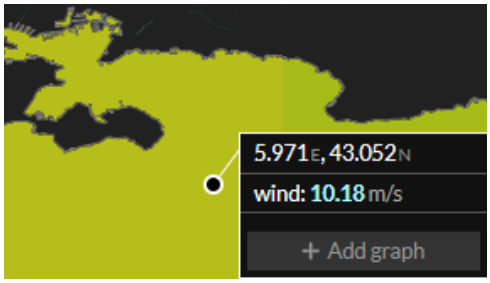

Figure 13: Wind (m/s) on October 16

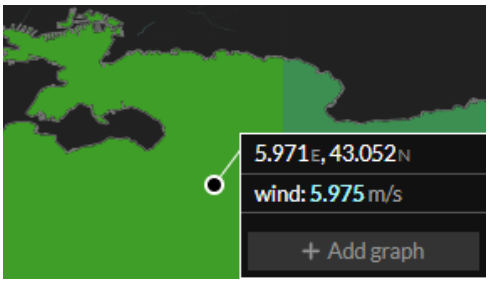

Figure 14: Wind (m/s) on October 18

The wind data, which are shown in Figure 13 and Figure 14 and used in this analysis, were sourced from the Marine Copernicus website, approximately for the Toulon Bay area on October 16 and October 18 at 09:00AM.

4 Conclusion

The field study conducted in Toulon Bay offered a unique opportunity to examine the interplay between surface and subsurface oceanographic processes in the Mediterranean Sea, using a combination of equipment and data analysis techniques. The results revealed a water column that reflects the region's complex hydrological characteristics, marked by sharp stratification and variability driven by atmospheric and oceanic forces. The CTD data captured the thermal and salinity gradients that define the Mediterranean's signature stratification, from warm, saline surface waters to cooler, denser depths. Spatial and temporal contrasts in temperature and salinity profiles not only demonstrated localized influences of weather, currents, and mixing but also underscored broader regional patterns tied to seasonal and annual variability. Comparisons with previous years highlighted a significant cooling of surface layers and sharper thermoclines in 2024, pointing to the possible influence of climatic factors on water column structure.

The drifter deployments added a dynamic dimension to the study, illustrating how surface currents and wave interactions are shaped by environmental conditions and the design of observational tools. The marked differences in drifter trajectories and velocities emphasized the interplay of wind, waves, and anchoring, providing a nuanced understanding of surface current behavior over time. Observations from multiple days illustrates the impact of weather patterns, with higher velocities on days of stronger winds underscoring the sensitivity of surface currents to atmospheric forcing.

Beyond these findings, the study underscored the value of integrating cutting-edge data processing tools with field measurements to generate actionable insights. By using algorithms to analyze trajectories and calculate velocities, the team was able to capture the subtle variations and dynamic patterns that define this marine environment. This approach offers a roadmap for future studies aiming to explore the Mediterranean's complex ecosystems or similar marine regions worldwide.

All in all, this investigation not only expanded our understanding of the Mediterranean Sea's physical and dynamic properties but also demonstrated the critical role of combining observational rigor with methodological innovation. The findings pave the way for future research into the implications of environmental change on oceanic systems, supporting efforts to sustainably manage and protect marine resources in the Mediterranean and beyond.